Journal of
Marine Science and Engineering

MDPI

Article

Utilizing Numerical Models and GIS to Enhance Information Management for Oil Spill Emergency Response and Resource Allocation in the Taiwan Waters

Chi-Min Chiu [1], Laurence Zsu-Hsin Chuang [2], Wei-Liang Chuang [1,*], Li-Chung Wu [3], Ching-Jer Huang [4] and Yinglong Joseph Zhang [5]

[1] Department of Marine Environment and Engineering, National Sun Yat-Sen University, Kaohsiung 80424, Taiwan
[2] Institute of Ocean Technology and Marine Affairs, National Cheng Kung University, Tainan 70101, Taiwan
[3] Coastal Ocean Monitoring Center, National Cheng Kung University, Tainan 701401, Taiwan
[4] Department of Hydraulic and Ocean Engineering, National Cheng Kung University, Tainan 70101, Taiwan
[5] Center for Coastal Resource Management, Virginia Institute of Marine Science, Gloucester Point, VA 23062, USA
* Correspondence: wlchuang@mail.nsysu.edu.tw

Abstract: This study aims to establish a comprehensive workflow for developing emergency response plans for both actual and scenario oil spill incidents in the Taiwan waters while addressing the resource allocation for oil spill containment as well. This workflow comprises two vital components. The first component involves the integration of numerical tools and observational data, which includes the incorporation of wind data from sources such as the National Centers for Environmental Prediction (NCEP) or meteorological stations. Additionally, it incorporates ocean current data simulated by the semi-implicit cross-scale hydroscience integrated system model (SCHISM) into the general NOAA operational modeling environment (GNOME) model, which is a new approach for this purpose. In order to assess the efficacy of this component, two distinct case studies were conducted. The first case study focused on an incident in a northern coastal area of Taiwan under open sea conditions, whereas the second case study examined an incident within a major commercial harbor in central Taiwan. The second component of this workflow involves creating oil risk maps by integrating the results from the first component with specific geographical factors into Google Earth. These oil risk maps serve multiple purposes. They offer real-time information to emergency response commanders regarding oil spill hazard prediction, and they also enable the effective development of emergency response strategies and disposal plans for potential oil spill incidents. This is achieved by generating risk maps for various scenarios using the approach outlined in the first component. Additionally, these maps assist in the assessment and planning of resource allocation for oil containment.

Keywords: oil spill; SCHISM; GNOME; GIS; risk map; emergency response

check for updates

Citation: Chiu, C.-M.; Chuang, L.Z.-H.; Chuang, W.-L.; Wu, L.-C.; Huang, C.-J.; Zhang, Y.J. Utilizing Numerical Models and GIS to Enhance Information Management for Oil Spill Emergency Response and Resource Allocation in the Taiwan Waters. *J. Mar. Sci. Eng.* **2023**, *11*, 2094. https://doi.org/10.3390/jmse11112094

Academic Editors: Giorgio Anfuso, Carlo Lo Re, Giorgio Manno, Rosa Molina and Francisco Asensio-Montesinos

Received: 23 September 2023
Revised: 23 October 2023
Accepted: 27 October 2023
Published: 31 October 2023

1. Introduction

Taiwan, located along significant shipping routes in East Asia, faces a high risk of oil spill incidents. Adverse weather conditions often contribute to ship collisions, groundings, or accidental spills during oil transportation operations, resulting in oil spill incidents in open sea areas. In order to address such incidents, Taiwan enacted the Marine Pollution Control Act in 1990 and has continuously enhanced its emergency response mechanisms for oil spills over the past two decades, keeping pace with technological advancements.

In the context of oil spill response, the timely dispatch and allocation of pollution control materials are crucial. However, the circumstances and extent of oil spill incidents vary and are subject to constant change. Allocating limited emergency materials effectively, in terms of location and quantity, requires the consideration of various factors such as local ocean currents, tides, wind speed and direction, environmental sensitivity levels, and risk assessments for potential oil spill impacts with varying time delays.

Oil weathering refers to the behavior of oil on the sea surface, including spreading, evaporation, dispersion, emulsification, dissolution, oxidation, sedimentation, sinking, and biodegradation [1,2]. The weathering process of oil spills is highly complex, influenced by variations in marine meteorological conditions. Numerically, simulating this process typically requires significant computational resources. However, advances in computer technology over the past two decades have facilitated the development of numerical models capable of describing the weathering process of oil spills [3–7].

Among the various factors influencing the simulation of oil spill dispersion on the sea surface, wind and currents play significant roles [8–10]. High-resolution numerical models for ocean currents can capture the changing characteristics of nearshore currents influenced by curved topography, improving the accuracy of oil spill dispersion predictions [11]. Remote sensing technology, such as X-band marine radar, is commonly used to detect the extent of oil spill diffusion on the sea surface, providing valuable information for establishing the initial area parameter in oil spill diffusion models [12,13]. By combining computer numerical models with X-band marine radar data, the accuracy of oil spill dispersion simulations can be enhanced [11].

Utilizing numerical models to simulate scenarios in open sea areas [14] and within harbors [15] provides crucial reference data for emergency response planning and resource allocation. Effective oil spill emergency response requires a comprehensive understanding of the affected maritime area's ecological environment, sensitive resources, and relevant geographic information [16–19]. Integrating these factors and establishing them on a web-based platform enables on-site emergency response commanders to rapidly access the latest information on oil spill incidents. This allows them to formulate initial emergency response strategies promptly. The generation of risk maps for oil spills in the maritime area further assists in emergency response planning and resource allocation.

Fernandes et al. [20] conducted an evaluation encompassing 19 oil spill models, which included both commercial and open-source variants. Among these models, the general NOAA operational modeling environment (GNOME) model received the highest rating. The GNOME model is an open-source tool developed by the Hazardous Materials Response Division (HAZMAT) of the National Oceanic and Atmospheric Administration Office of Response and Restoration (NOAA OR&R), as detailed by Duran et al. [21]. Notably, this model accommodates diverse environmental conditions, such as wind fields and ocean currents, which can be derived from observations or other numerical tools. In light of these advantages, GNOME has been selected as the oil spill model for this study. Ocean currents play a pivotal role in propelling the dispersion of oil spills. Integrating GNOME with other ocean models to acquire reliable ocean current data is a prevalent practice. Recently, the semi-implicit cross-scale hydroscience integrated system model (SCHISM), developed by the College of William & Mary [22–24], has gained widespread popularity as a numerical tool for simulating ocean currents in various applications related to environmental fluid mechanics. Nonetheless, the effectiveness of integrating GNOME and SCHISM has not yet been assessed. This study endeavors to address this critical gap.

In addition to establishing oil spill simulation using GNOME and SCHISM, this study aims to create a comprehensive workflow for developing emergency response plans for both real and scenario oil spill incidents in the waters around Taiwan. This workflow also includes addressing resource allocation for oil spill containment. It comprises two main components. The first component focuses on oil spill simulation, utilizing observational data, SCHISM, GNOME, and a numerical tool for wind simulation. The second component is dedicated to generating oil risk maps. It involves integrating the outcomes from the first component with specific geographical factors and visualizing them within Google Earth.

In order to evaluate the effectiveness of the two components, two distinct oil spill incidents in the Taiwan waters were chosen as case studies. The first case study is centered around the TS Taipei oil spill incident, which is a well-documented maritime accident with a known spill location and time. The second case study pertains to an oil spill incident within Taichung Port, originating from an unknown source, where both the spill location and time are uncertain. Following these case studies, oil risk maps for both scenarios were generated, and the subsequent discussions revolve around their applications in planning emergency response and resource allocation for oil containment.

2. Numerical Tools and Observational Data

2.1. Oil Spill Simulation

Oil spill models play a crucial role in assessing risks and impacts on natural resources resulting from actual and potential spills. Simulation results are essential in guiding the development of strategies for oil spill planning and response [25]. Typically, oil spill models employ the random walk method to predict the transport of surface oil slicks [26,27]. Two-dimensional oil spill models utilize wind and current velocities, which can be either constant or variable, to simulate the movement of surface oil slicks.

In this study, the general NOAA operational modeling environment (GNOME) model was utilized for oil spill simulation. This 2D Eulerian-Lagrangian model has been widely employed in marine, coastal, and riverine regions [28–30] to track the movement of oil slicks [31,32]. When an oil spill incident occurs in the ocean, the US NOAA utilizes GNOME to simulate the dispersion and drift trajectory of the oil spill on the sea surface [30]. The simulation results provide valuable guidance for the government in dealing with oil spills and formulating emergency response strategies. GNOME is extensively used worldwide [33] for oil spill incident simulations and has been recognized as the top-performing oil spill model by the Joint Research Centre of the European Commission [20].

Wind kinematics are essential inputs for the oil spill model. In this study, the primary source of wind kinematics data was obtained from observational data acquired at weather stations situated in the vicinity of the regions of interest. In the case study of the TS Taipei oil spill incident, we extended the oil spill simulation to incorporate the simulated wind kinematics generated by the National Centers for Environmental Prediction (NCEP) model. The comparison between the use of observed and simulated wind kinematics enables us to assess the NCEP model's suitability for local coastal applications.

Ocean hydrodynamics play a crucial role in the dispersion of oil spills, resulting from the complex interaction of wind, currents, bathymetry, and coastal topography. For ocean hydrodynamics, SCHISM (semi-implicit cross-scale hydroscience integrated system model) was employed in the present study. Within SCHISM, the Navier-Stokes equations are solved in a hydrostatic form using a semi-implicit finite-element/finite-volume method, and momentum advection is solved using an Eulerian-Lagrangian method [34]. SCHISM utilizes mixed triangular-quadrangular unstructured meshes for horizontal considerations and a flexible co-ordinate system called localized sigma co-ordinates with shaved cell (LSC^2) to solve the pressure gradient and reduce the pressure gradient error (PGE) in the vertical [35]. It is essential to highlight that vertical mesh smoothing is not required when implementing the LSC^2 method in areas characterized by steep bathymetric slopes or highly variable depths. This circumvents the numerical stability issue that many ocean hydrodynamic models typically face in such areas.

Moreover, SCHISM accounts for air-sea exchange and can be coupled with the wind wave model-III [36,37] to enhance the accuracy of predicted coastal hydrodynamics. The utilization of unstructured triangular meshes in SCHISM enables the accurate representation of the complex coastal topography. This feature is particularly advantageous for conducting oil spill simulations on the northeast coast of Taiwan, owing to bays and rugged coastlines [11,38]. It facilitates precise simulations of the variable ocean currents appearing in these areas.

Windage is a critical factor that affects the movement of surface oil spills. The GNOME model recommends a default wind factor ranging from 1% to 4% [39,40]. In this study, a wind factor of 3% was adopted based on analytical derivation and empirical observation [39]. The diffusion coefficient is another significant factor associated with the random spreading of spilled oil. A default diffusion coefficient of 100 m^2/s was utilized, considering its extensive use in GNOME for simulating the movement of spilled oil [30,31,41]. For large-scale simulations, such as those in coastal or open sea areas, the second version of the climate forecast system re-analysis (CFSv2) models [42,43] can be employed to obtain surface wind data for the GNOME model. For small-scale simulations, such as those in harbors, it is recommended to utilize wind data collected from nearby buoys and coastal stations. This data typically provides sufficient spatial resolution for accurate modeling and analysis.

It is essential to mention that SCHISM and GNOME have been extensively documented in the literature across various applications. In order to avoid redundancy, readers are encouraged to refer to the previously mentioned references for more comprehensive information and related mathematical expressions.

2.2. X-Band Marine Radar

Remote sensing technology plays a crucial role in monitoring and observing oil spills in both open waters and coastal areas [2,13]. It provides real-time information and accurate spatial mapping of spilled oil, as well as continuous 24 h monitoring of sea surface currents, waves, and the location and movement of oil slicks. Various remote sensing technologies, such as aircraft, satellites, and radar, can be utilized to detect oil slicks of different sizes. For spills in open waters, aircraft or satellites are commonly used to assess the distribution of oil slicks [44]. For coastal spills, the utilization of X-band marine radar, characterized by superior spatial and temporal resolution, is the preferred option. X-band marine radar offers real-time, convenient, fast, and cost-effective oil slick detection compared to other methods, such as synthetic aperture radar [45,46].

In this study, X-band marine radar was primarily employed to evaluate the initial extent of the oil slick on the sea surface, offering essential initial conditions for the oil spill simulation. Among the two oil spill incidents investigated in this study, only the TS Taipei oil spill incident incorporated the use of X-band marine radar. For the other incident that occurred within the harbor, X-band marine radar was not available. This issue was addressed by extrapolating the initial oil slick extent according to the information from media reports.

2.3. GIS

GIS (geographic information system) has gained widespread recognition as an excellent management tool for response and planning, damage assessment, and resource allocation evaluation in oil spill incidents [47–49]. It provides users with a universal and user-friendly interface for analyzing the impacts of oil spills. One key advantage is the integration of oil spill modeling and GIS, which facilitates the creation of dynamic and interactive platforms, enabling decision-makers to visualize and explore oil spill scenarios in a spatial context [50]. This integration leads to quicker decisions and more accurate estimation of the magnitude and trajectory of oil spills. Furthermore, it can establish oil spill risk maps for marine environments, offering valuable reference information for emergency response plans, the design of rescue equipment, and accident mitigation. These maps also serve as useful references for risk assessment and management [51,52], which the present study aims to generate for both case studies.

In this study, Google Earth was selected as the GIS tool in order to eliminate the need for specialized GIS software (QGIS Desktop 3.16.16 & Python 1.2), as it is accessible across various computer operating systems and mobile devices. In order to create the oil spill risk maps, the simulated results and relevant information, such as environmentally sensitive areas, are initially converted into the KML file format. Subsequently, these data in the KML format can be directly imported into Google Earth, enabling a visual representation and analysis of the potential impact of oil spills.

3. TS Taipei Oil Spill Incident on the North Coast of Taiwan

3.1. Overview of the TS Taipei Oil Spill Incident

The waters surrounding Taiwan hold significant international importance, serving as a crucial shipping route for a substantial number of oil tankers and cargo vessels. During the winter season, the northeast area of Taiwan is significantly affected by prevailing northeast monsoon winds, which occasionally lead to ship grounding incidents [53]. These incidents can lead to hull breakage and subsequent oil spills. One notable incident occurred on 10 March 2016, when the cargo vessel TS Taipei lost power and ran aground near the shore in Shimen, New Taipei City, approximately 300 m off the coast. This coastal area boasts rich fishery resources and sustains diverse ecosystems. Consequently, any oil spill incident in this vicinity would exert a significant influence on the local marine environment. Therefore, the TS Taipei oil spill incident was chosen as a distinctive case study in our current simulation, focusing on the oil spill scenario in a coastal region under open sea conditions. Moreover, besides comparing the observed extent along the coastline, we undertook an assessment of the potential risks and consequences of oil spills in the region.

The local computational domain spans a horizontal area of 71 km by 32 m, as shown in Figure 1, and unstructured triangular meshes were utilized. Note that there are 118,132 horizontal grid points in this setup. Figure 2 demonstrates the nearshore flow fields dominated by tidal currents near the site of the TS Taipei incident, simulated using SCHISM, during flood tide and ebb tide, respectively. The flow patterns reveal the intricate circulations arising from the interaction between the prevailing currents and the jagged coastlines. This outcome not only suggests the suitability of the current mesh deployment and SCHISM's capability to resolve the intricate nearshore current patterns resulting from complex coastal topography but also signifies the potential complexity of oil spill dispersion in the surrounding coastal regions.

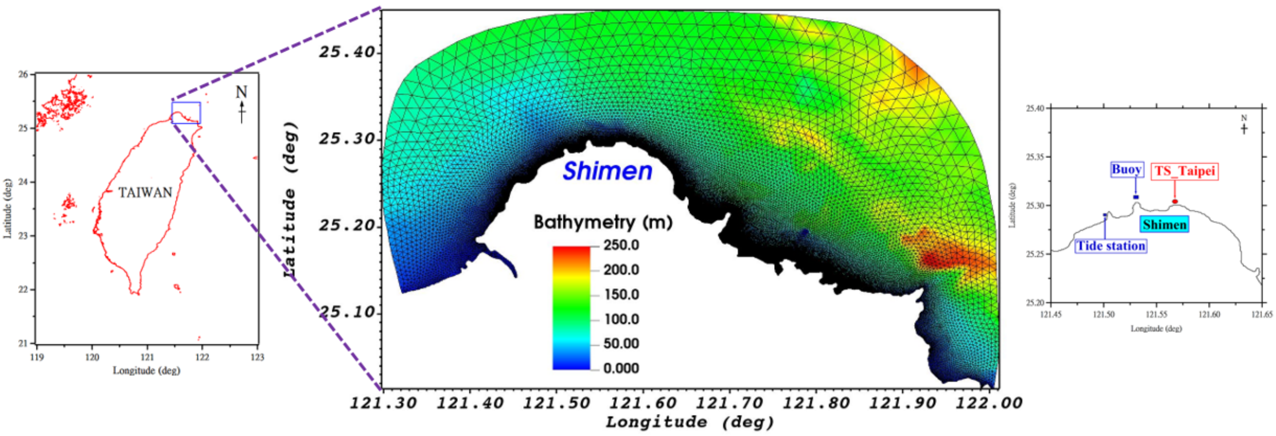

Figure 1. Horizontal computational domain filled with unstructured triangular meshes for the simulation of the case study of the TS Taipei oil spill incident. Locations of the incident site, buoy, tidal station, and the nearby district of Shimen are displayed as well.

It is worth noting that these circulations can potentially trap oil spills within bays, which can be advantageous for oil containment and cleanup. However, it is important to recognize that this phenomenon may have a more pronounced impact on the coastal ecological environment. On the contrary, if oil slicks drift offshore, they can disperse to nearby coastlines through tidal currents, leading to a wider-reaching impact on the marine environment.

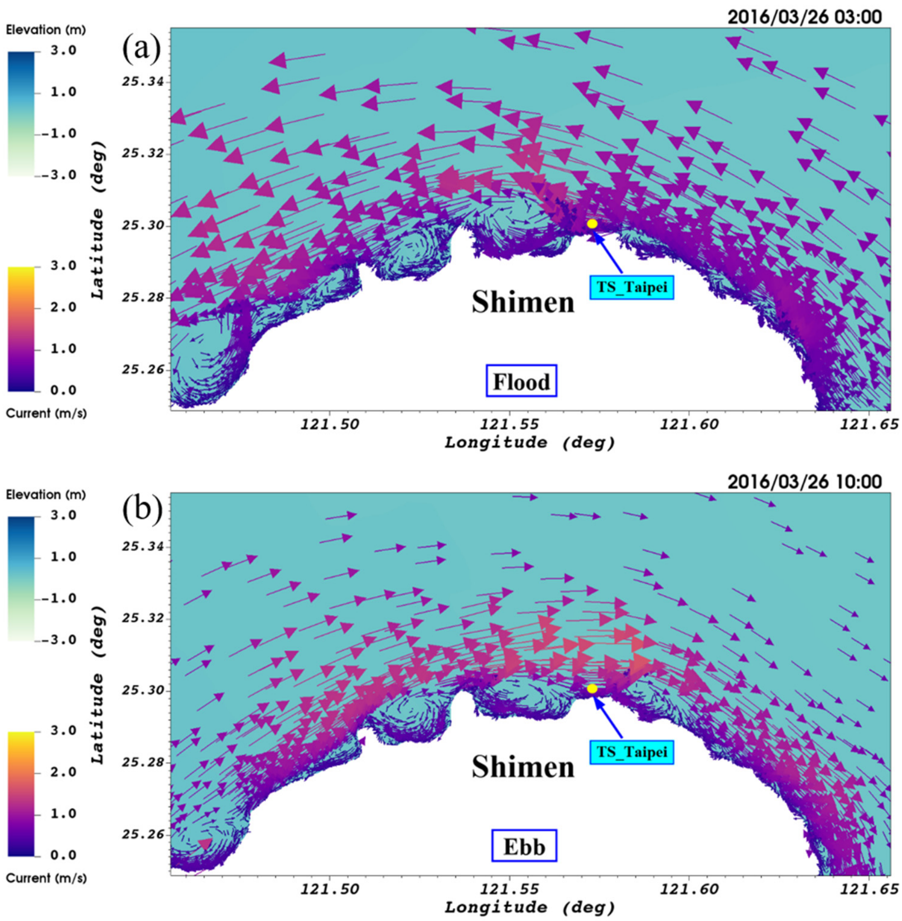

Figure 2. Current flow fields simulated by SCHISM during flood tide (**a**) and ebb tide (**b**) in north-eastern Taiwan during March 2016.

Following the TS Taipei incident on 26 March 2016, a research team from the Coastal Ocean Monitoring Center at National Cheng Kung University deployed an X-band marine radar to observe the extent of the oil spill on the sea surface. For a comprehensive understanding of the application of X-band marine radar in oil spill detection and its specific application in observing the TS Taipei oil spill incident, please consult the work by the authors of [11]. The detected extent of the oil spill, represented by the black shaded area in Figure 3, covers an area of approximately 1 km^2. This observation provides valuable input for the initial oil spill extent in the oil dispersion simulation.

3.2. Validation

Both SCHISM and NCEP were utilized to generate environmental inputs for GNOME in this case study. Validation for both models was conducted by comparing their simulated results with observational data from the Fuguei Cape buoy (for wind speed and direction) and the Lingshanbi tidal station (for sea water level), for which their locations are marked in Figure 1.

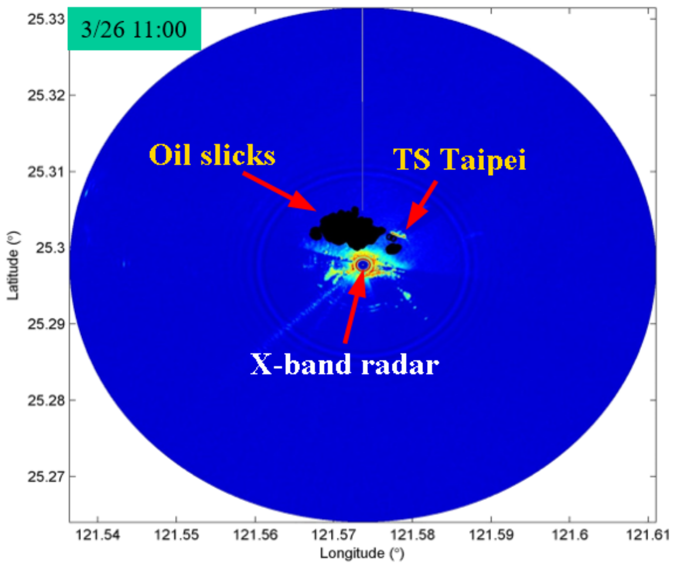

Figure 3. Surface oil slick was detected by X-band marine radar (area in black) at 11:00 a.m. on 26 March 2016. The black color in the picture represents the extent of the oil spill's spread range.

Figure 4 presents the validation result for NCEP. In Figure 4, the time series reveals that during the period from 21–28 March 2016, the prevailing wind direction was predominantly from the northeast, accompanied by high wind speeds. Starting from 29–31 March, the dominant wind direction began to change. The comparison of both datasets shows a disparity in magnitude, which can be attributed to the limited spatial resolution of the computational grids used by NCEP for such local coastal regions. Note that NCEP is a global weather model with a spatial resolution of 0.205 degrees (approximately 22.76 km). Nonetheless, it is crucial to acknowledge that the consistent trends and differences of less than one order of magnitude suggest that the wind fields predicted by NCEP in this region during the period of interest can be considered reliable for confidently predicting the extent and drift direction of oil spills.

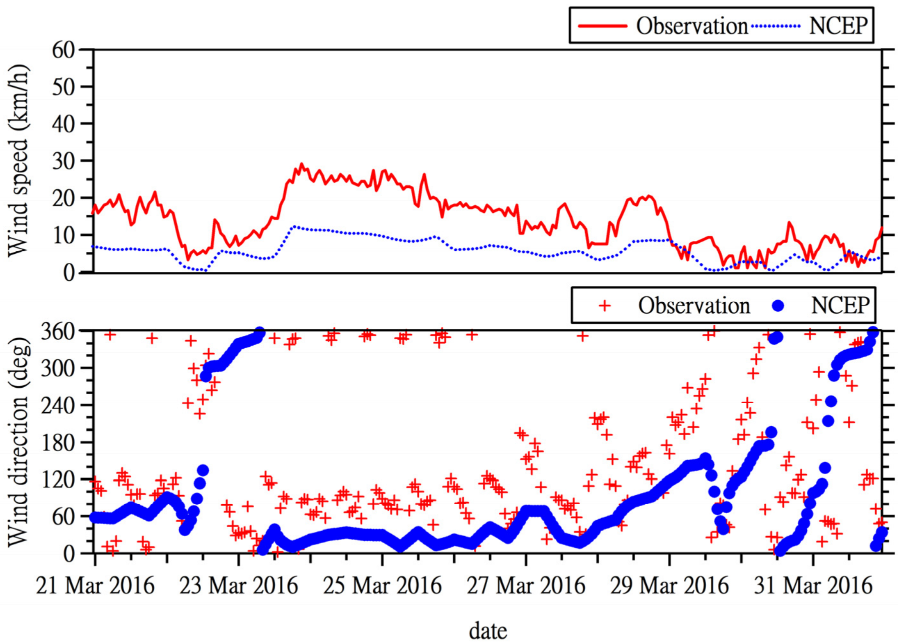

Figure 4. Comparison between the prediction by NCEP and the observation collected by the Fugui Cape buoy for wind speed and wind direction.

Figures 5 and 6 present the validation results for SCHISM. Figure 5 displays the validation of sea water level for the period from 21 March–30 April 2016, showing a strong agreement between the simulated and observed data. Figure 6 presents the validation of current velocity and direction from 1–11 April 2019 and demonstrates the reliability of SCHISM in representing variations in currents off the northeast coast of Taiwan. The reason we did not conduct validation for the same period in 2016 is due to the unavailability of observational data from the Fuguei Cape buoy during that time. However, given the similarities in seasonal ocean currents, the validation results presented in Figure 6 provide a reasonable basis for demonstrating the effectiveness of SCHISM in predicting current velocity and direction for the TS Taipei oil spill incident.

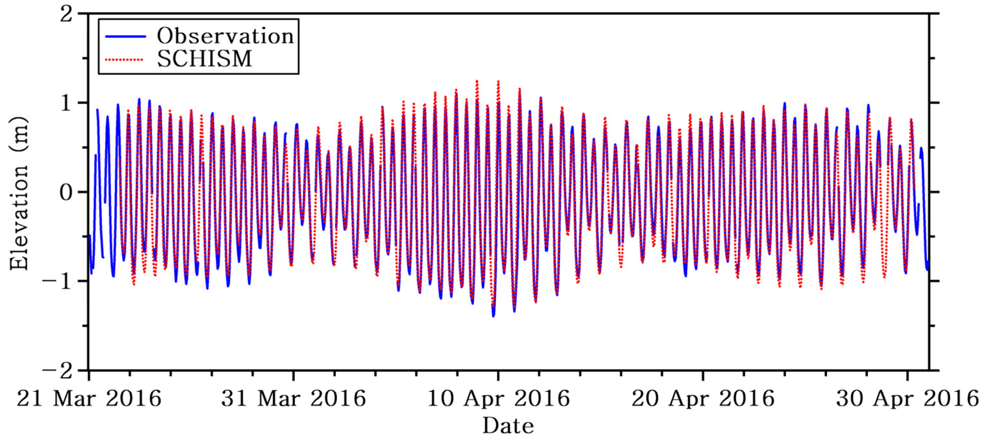

Figure 5. Comparison of sea water level between the simulated result obtained from SCHISM and the measurement recorded at the Linshanbi tidal station during the period of 21 March to 30 April 2016.

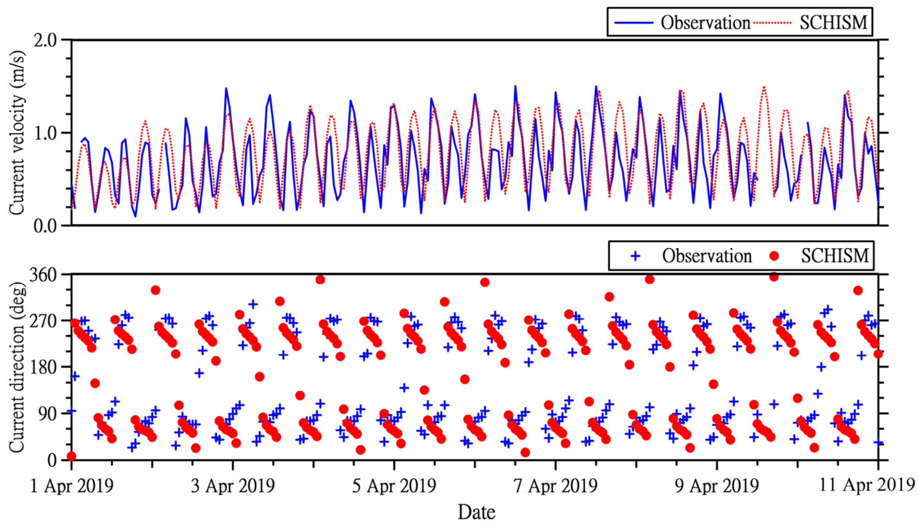

Figure 6. Comparison between the prediction by SCHISM and the measurements collected at the Fuguei Cape buoy for current velocity and current direction during the period of 1–11 April 2019.

3.3. Oil Spill Simulation Result

Table 1 provides the main parameters employed in the GNOME simulation for the TS Taipei oil spill incident. The oil spills in this incident consisted of fuel oils commonly used for ships and vessels. The initial condition for the oil spill area and location were obtained from the X-band marine radar detection of the oil slick on the sea surface, with an estimated area of approximately 1 km^2 (as depicted in Figure 3). The color of the oil slick on the sea surface was described as brown to black, indicating an oil film thickness greater than 0.1 mm according to ITOPF-TIP1 [54,55]. The estimated quantity of oil released was approximately 60 metric tons. The start time for the oil spill on the sea surface was determined based on the moment of oil slick detection by the X-band marine radar, resulting in an instantaneous oil spill duration of 0 hr. In the present simulation, we have defined two cases using different sources of wind data: Case I relies on predictions from NCEP, while Case II utilizes observational data collected from the Fuguei Cape buoy.

Table 1. Parameters for the simulation of the TS Taipei oil spill incident.

Parameters	Description
Oil type	Fuel oil
Spill area	About 1 km^2
Amount released	60 KL
Release start	At 11 am on 26 March 2016
Age at release	0 h
Splots	1000
Diffusion coefficient	10 m^2/s
Current	SCHISM
Wind	NCEP and Buoy (Case I and Case II)
Simulation duration	1 day, 3 days, and 34 days

Figures 7 and 8 present the simulation results at four moments for Case I and Case II, respectively. Note that each Splot in the figures corresponds to an individual oil particle point [40]. The oil distribution is visualized with red triangles representing oil slicks adhered to the coast and green dots representing oil floating on the sea surface. Additionally, the movement of oil on the sea surface was influenced by the combined forces of 100% surface current velocity and 3% wind speed [39]. The GNOME model suggests using windage values of 1% to 4% [30,56], and in this study, windage was set at 1% to 4% in the GNOME model.

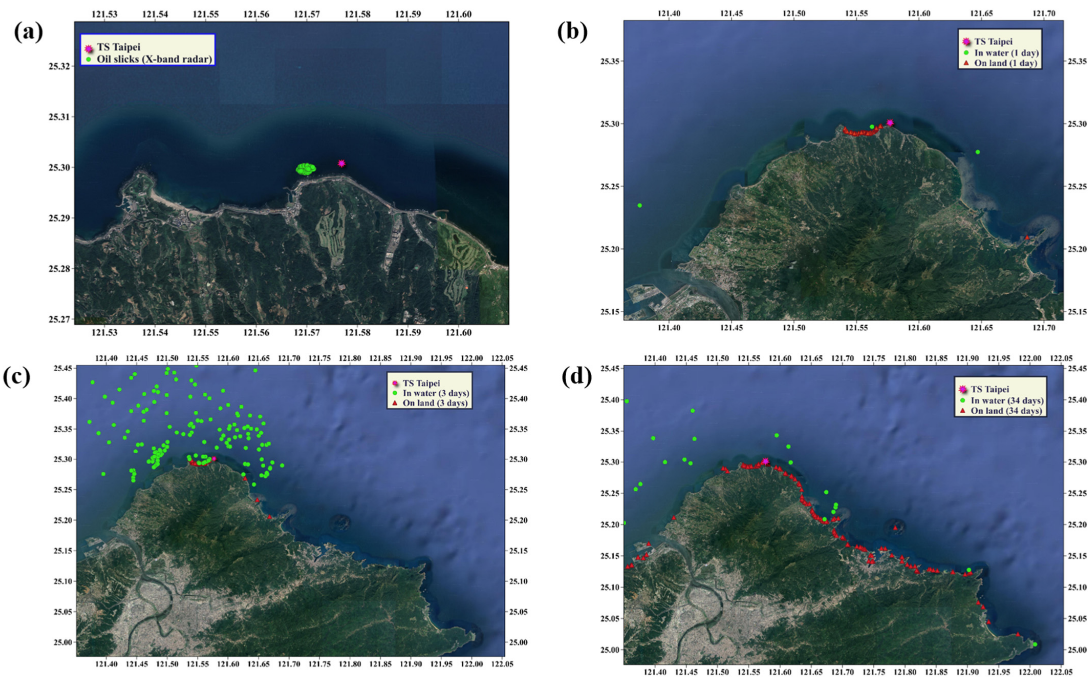

Figure 7. (**a**) Initial oil slicks detected by X-band marine radar and the simulated oil spills after (**b**) 1 day, (**c**) 3 days, and (**d**) 34 days for Case I. Note that the purple symbol denotes the site TS Taipei ran aground, and the green and red symbols indicate oil slick drifting on the sea surface and oil slick adhering to the coast, respectively.

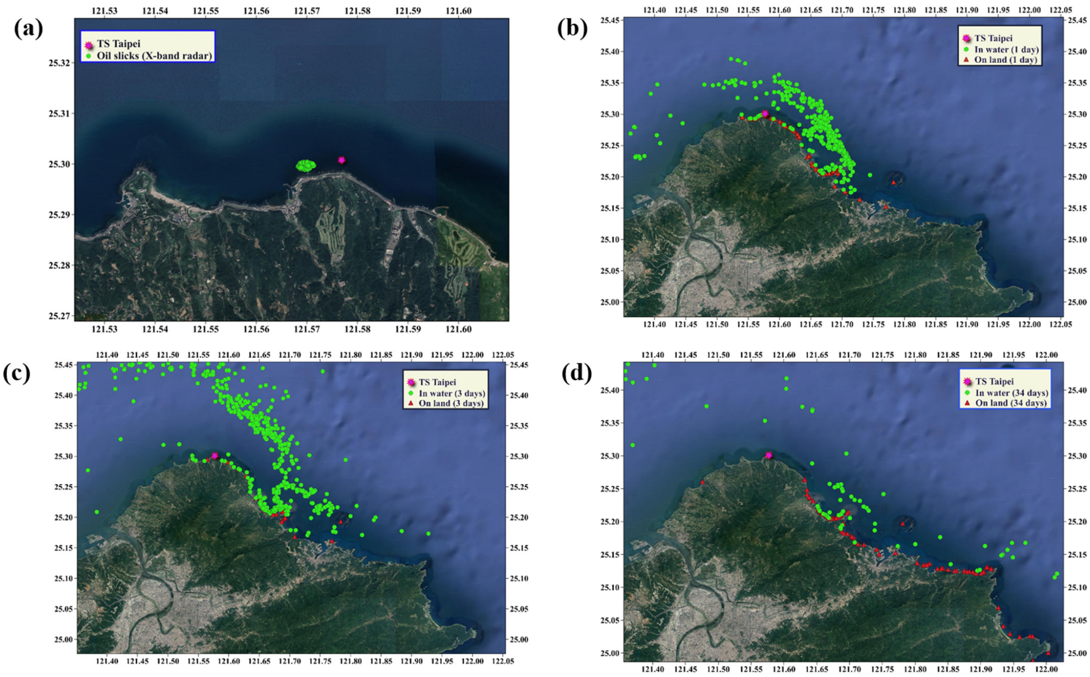

Figure 8. (**a**) Initial oil slicks detected by X-band marine radar and the simulated oil spills after (**b**), 1; day, , (**c**) 3 days, and (**d**) 34 days for Case II. Note that the purple symbol denotes the site TS Taipei ran aground, and the green and red symbols indicate oil slick drifting on the sea surface and oil slick adhering to the coast, respectively.

In Case I, following the oil spill incident for 1 day, as depicted in Figure 7b, the majority of the oil had spread across the Shimen district, with a portion of it adhering to the coastline, affecting a coastline stretch of approximately 4.3 km. Figure 7c vividly illustrates that after 3 days from the onset of the incident, the oil had dispersed and drifted over a significantly broader area around the Shimen district. This dispersion was primarily driven by the combined effects of winds and tidal currents. A substantial amount of oil slicks had adhered to the coastline, impacting an extensive coastline length of approximately 15 km. In Figure 7d, the simulated oil spill dispersion is presented 34 days after the incident. The result indicates that the oil spill had a significant impact on the entire northeast coast of Taiwan. Remarkably, some oil had even drifted into the western waters of Taiwan. The length of the coastline affected by the oil spill had escalated considerably, extending to approximately 98 km.

In Case II, 1 day after the oil spill incident, as shown in Figure 8b, the oil primarily dispersed in the region between Shimen and Keelung, with some adhering to the coastline, affecting approximately 38 km of shoreline. After 3 days, as demonstrated in Figure 8c, the oil continued to spread primarily between Shimen and Keelung, and it appeared that southwest winds were predominantly influencing the oil movement. The impacted coastline remained at approximately 38 km. By the 34th day after the incident, as displayed in Figure 8d, there was a noticeable reduction in oil on the northeastern sea surface but an increase in oil slicks adhered to the coastline. The affected coastline extended from Tamsui in the west to Sandiaojiao in the east, covering approximately 85 km.

In order to assess Case I and Case II, we referred to a survey conducted by the Environmental Protection Agency in Taiwan, henceforth referred to as Taiwan EPA. Figure 9 displays the surveyed coastlines impacted by the TS Taipei oil spill incident 34 days later. Upon comparison with the survey result, Case I demonstrates better performance. This suggests that the use of simulated wind data with higher spatial resolution is more suitable for this oil spill scenario. Furthermore, it is important to highlight that, in the aftermath of the TS Taipei oil spill incident, the Taiwan EPA promptly initiated an emergency response, mobilizing a range of oil cleanup equipment and personnel to reduce the impact on the coastline [52]. Consequently, the actual length of the affected coastline was mitigated due to these cleanup efforts.

Figure 9. The oil spill extent along the northeast coast of Taiwan, as surveyed by the Taiwan EPA on 29 April 2016, during the TS Taipei oil spill incident. The blue rectangle in the top-left of the Taiwan map denotes the area visible on Google Earth.

In this case study, a further step was taken to simulate the weathering process of the TS Taipei oil spill incident over a 34-day period for Case I only, and the result is presented in Figure 10. Note that the weathering process includes the rate of change in floating oil on the sea surface, the rate of change in oil reaching the coast, and the rate of change in evaporated oil. In Figure 10, the abrupt change at the initial stage was primarily caused by the northeast wind, leading to the drift of oil toward the coastline. Shortly after 2 h of simulation, at 1 p.m. on 26 March, the amount of oil on the sea surface decreased from 100% to 16.7%, whereas the quantity of oil reaching the coast rapidly increased from 0 to 80.8%. However, after 3 p.m. on 29 March, due to a shift in wind direction, some oil near the coast was carried offshore by the wind. Consequently, the quantity of oil on the sea surface gradually increased, whereas the quantity of oil on the coastline exhibited a decreasing trend.

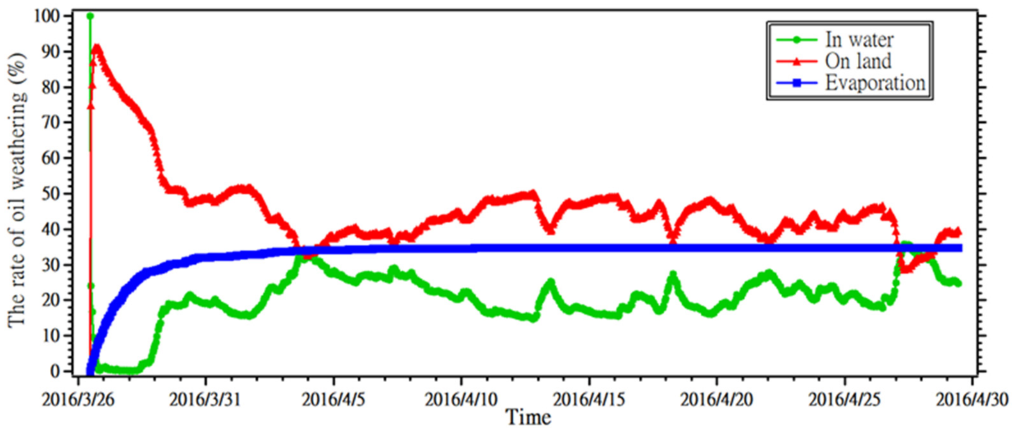

Figure 10. Simulated time series of weathering process over a period of 34 days for Case I.

4. Unknown Oil Spill Incident in Taichung Port

4.1. Overview of the Taichung Port Oil Incident

Taichung Port, situated in the central western area of Taiwan, functions as both an international commercial port and a hub for the offshore wind industry, encompassing construction, operation, and maintenance activities. Given the more frequent shipping activities in recent years, the potential risk of oil spills in the port has become a rising concern. Of particular significance is the northern area of Taichung Port, which adjoins the Gaomei Wetland Nature Preserve. Any oil spill incident in the port has the potential to adversely impact the ecological integrity of the wetland. On 19 October 2018, as depicted in Figure 11, an unknown oil spill incident occurred in Taichung Port. In order to precisely numerically model the oil dispersion within the harbor, enhancements were implemented to increase the spatial resolution of SCHISM. This improvement allows for capturing variations in flow velocity within the intricate topography of the area. Regarding wind data, the spatial resolution of the NECP-CFESv2 wind field is 0.205 degrees (approximately 22 km), which does not adequately represent the wind variations within the port. As a result, wind data collected from the observation station situated within the port were used as the input.

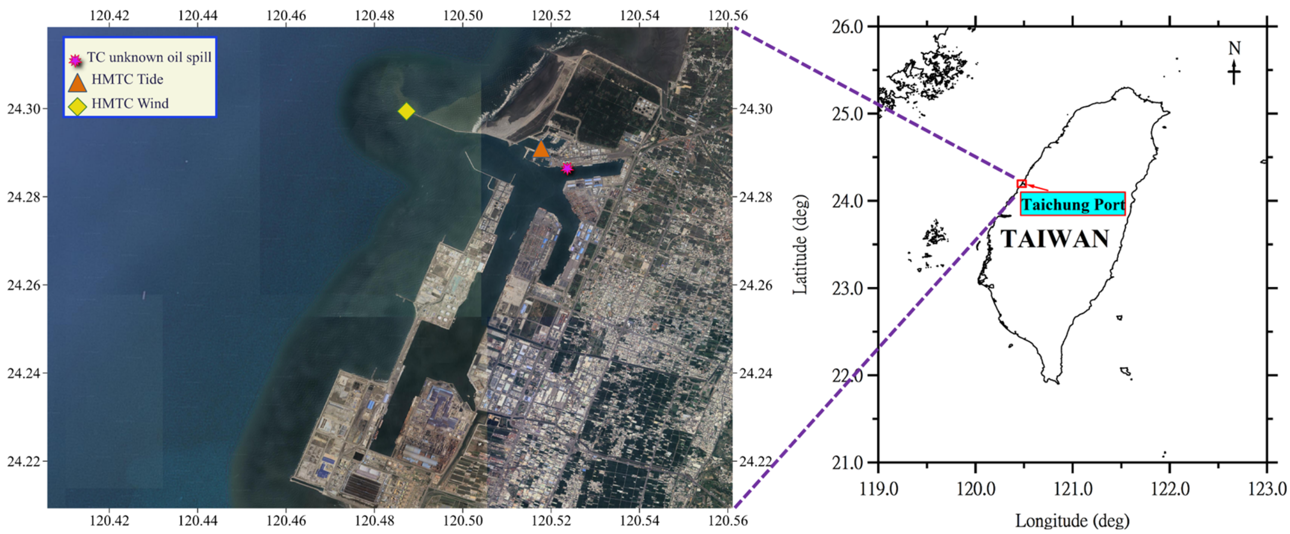

Figure 11. The location of the unknown oil spill incident within Taichung Port, along with the tidal station (HMTC Tide) and the meteorological station (HMTC Wind) deployed by TPRC.

The local computational domain covers a horizontal area of 110 km by 60 km, as shown in Figure 12, and unstructured triangular meshes were employed. Note that this setup comprises 20,000 horizontal grid points, and the smallest mesh size within the harbor is 20 m. When compared to Figure 1, it is evident that the bathymetry variation around Taichung Port is relatively gentle, with the slopes perpendicular to the coastline changing gradually.

Figure 13 illustrates the nearshore flow patterns that resulted from the tidal currents around Taichung Port. These simulations were conducted using SCHISM, capturing the conditions during flood tide and ebb tide. The presence of distinct circulations near the harbor entrance, resulting from the interaction between topography and ocean currents, is quite evident. During ebb tide, the current direction within the harbor displayed a northeast-to-southwest pattern, whereas the offshore flow exhibited a parallel alignment with the coastline. Similar flow patterns were observed during flood tide but in opposite directions.

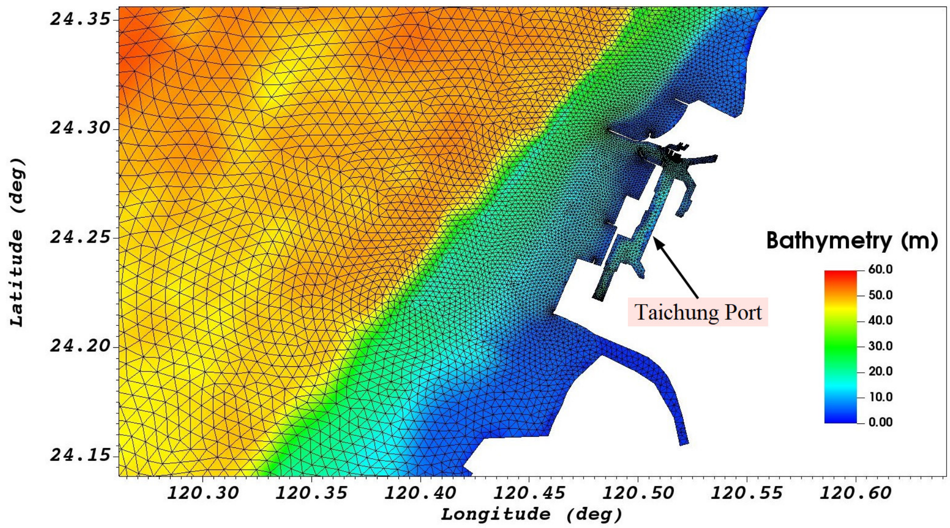

Figure 12. Horizontal computational domain filled with unstructured triangular meshes for the simulation of the Taichung Port incident.

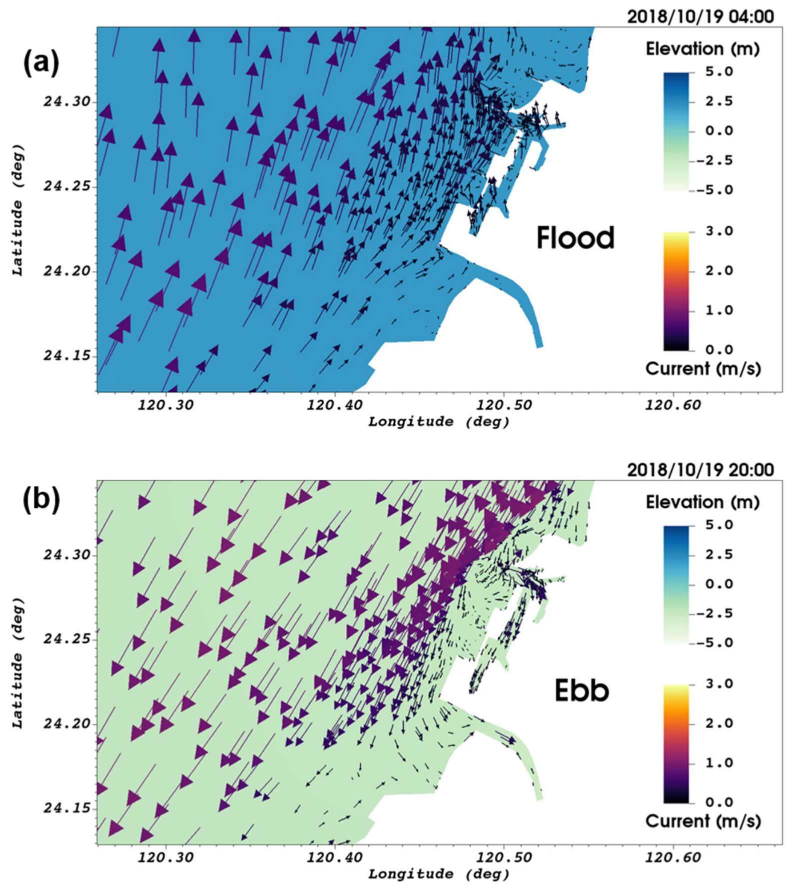

Figure 13. Current flow fields simulated by SCHISM during (**a**) flood tide and (**b**) ebb tide around Taichung Port during October 2018.

4.2. Validation

In this case study, SCHISM was exclusively used to generate environmental inputs for GNOME. For the purpose of validation, a comparison of sea water level was made between the simulated result and the observational data obtained from a tidal station named HMTC Tide (as shown in Figure 11). Note that this tidal station is managed by the Taichung Port

Research Center (TPRC). Figure 14 presents the validation result for a specific period in October 2018, coinciding with the duration of the unknown incident. The alignment in both magnitude and phase serves as a clear indication that SCHISM can effectively model ocean hydrodynamics in this region.

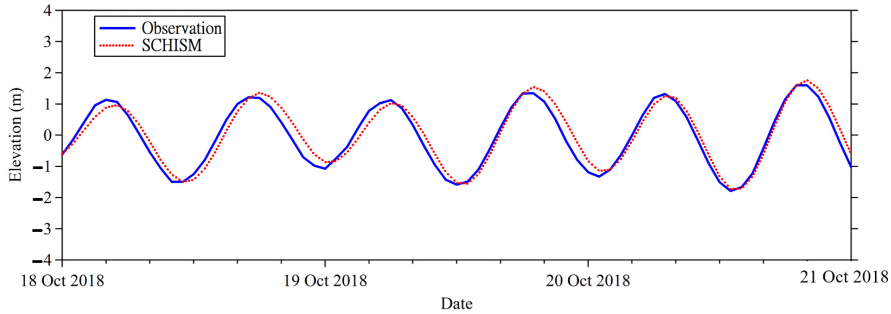

Figure 14. Comparison of sea surface elevation between the simulated result obtained from SCHISM and the measurement recorded at the HMTC Tide station.

4.3. Oil Spill Simulation Result

Table 2 provides the major parameters employed in the GNOME simulation for the unknown oil spill incident in Taichung Port. For the initial location of the oil spill, a spot between piers North 2 and North 3, as displayed in Figure 11, was chosen according to the media reports. The oil spill incident initially occurred at approximately 8:30 a.m. on 19 October 2018. Due to the absence of specific details for this incident, a scenario was formulated by referencing this with the TS Taipei oil spill incident described earlier. The scenario simulation assumed a total volume of 30 barrels of fuel oil being spilled, with the oil being continuously released over a period of 1 h. The simulation covered a time span of 12 h.

Table 2. Parameters for the simulation of the Taichung Port oil spill incident.

Parameters	Description
Oil type	Fuel oil
Spill location	Latitude: 24°17′12.6″ N Longitude: 120°31′33.2″ E
Amount released	30 KL
Release start	At 8:30 am on 19 October 2018
Age at release	1 h
Splots	500
Diffusion coefficient	10 m^2/s
Current	SCHISM
Wind	Meteorological station
Simulation duration	12 h

In the GNOME simulation, the input wind data were obtained from observational data collected at the meteorological station managed by TPRC as well, denoted as HMTC Wind in Figure 11. Figure 15 provides a rose chart and time series of the wind data for October 2018, encompassing the timeframe of the oil spill incident. The wind data reveals that, in October, wind speeds were predominantly greater than 10 m/s, with the primary wind direction originating from the north-northeast. Note that hourly wind data were employed in the simulation.

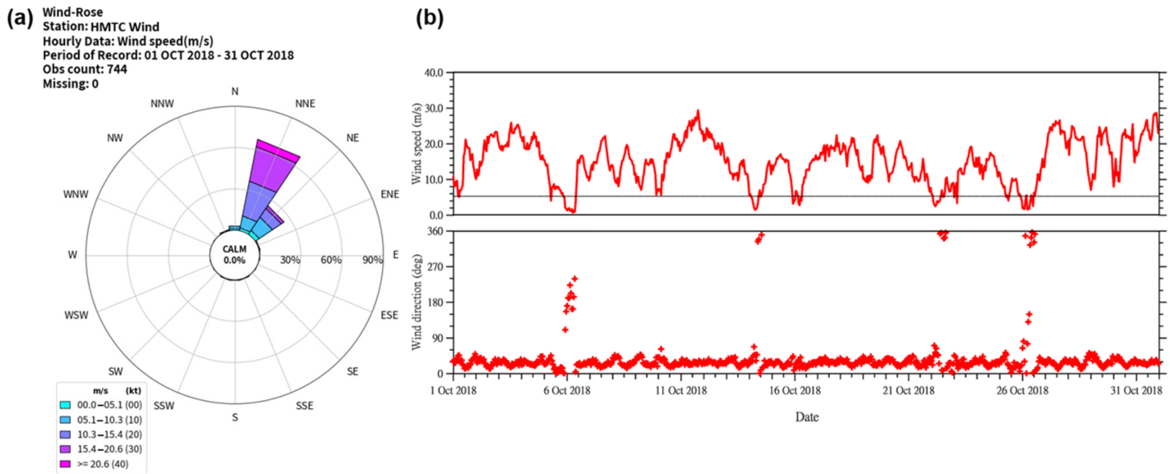

Figure 15. Observation of wind speed and wind direction recorded at the HMTC wind station in October 2018. (**a**) Rose chart and (**b**) time series.

Figure 16 presents the results of the scenario simulation carried out 5 h and 12 h following the oil spill incident. In this figure, the red triangles symbolize oil slicks adhered to the seawalls in Taichung Port, while the green dots represent oil slicks drifting within the harbor.

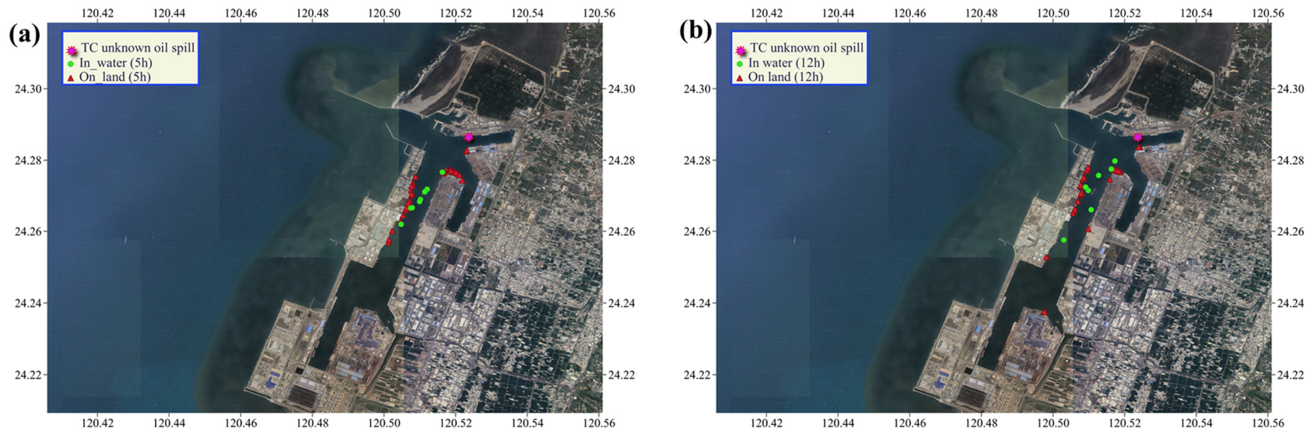

Figure 16. Simulated oil spills within Taichung Port after (**a**) 5 h and (**b**) 12 h.

During the entire simulation period, the dominant wind direction remained north-northeast, with wind speeds consistently exceeding 10 m/s. This prevailing wind pattern was identified as the primary factor driving the oil slicks in a southwest direction, eventually causing them to adhere to the western pier of Taichung Port. The influence of tidal currents on the oil dispersion within the harbor was insignificant. The oil spills were effectively contained within Taichung Port, preventing any impact on the coastal environment in the vicinity of Taichung Port.

According to [2], in the case of oil spills in open waters, if the wind speed exceeds 5.6 m/s, wind becomes the primary factor influencing the direction of oil spill drift. Based on the present simulation result, this conclusion seems applicable to the oil spills within the harbor area. Moreover, it is noteworthy that the simulation result after 12 h agrees with media reports, further reinforcing the conclusion that wind is the primary factor influencing the Taichung Port oil spill incident, as well as similar incidents of this nature.

It is important to highlight that the Taichung Port Authority and Taichung Environmental Protection Bureau swiftly executed emergency response measures in response to the oil spill incident. By the evening of 19 October, these efforts had effectively controlled the oil contamination, preventing it from spreading beyond Taichung Port and thereby minimizing the potential impact on the Gaomei wetland.

5. Information Establishment for Emergency Response

5.1. Oil Spill Risk Map

Oil spill risk maps are generally created through GIS by integrating various geographical factors, such as simulated oil dispersion, environmental features, ecologically sensitive areas, and important facilities. In the present study, oil spill risk maps for both case studies were created by incorporating specific geographical data within Google Earth. These data encompass geographical information of importance, including oil spill simulation results, environmental features, and ecologically sensitive areas, all of which are detailed in Table 3. The oil spill risk maps for the TS Taipei incident and the Taichung Port incident are displayed in Figures 17 and 18, respectively.

Table 3. Classification and icon representations of GIS objects in oil spill risk maps.

Class	GIS Object	Icon
Oil spill simulation result	Oil spill location	✸
	Oil in water	●
	Oil on land	▲
Environmental feature	River	
	Fishing port	●
Ecologically sensitive area	Exclusive fishing right	
	Artificial reef	
	National scenic area	
	Wetland	

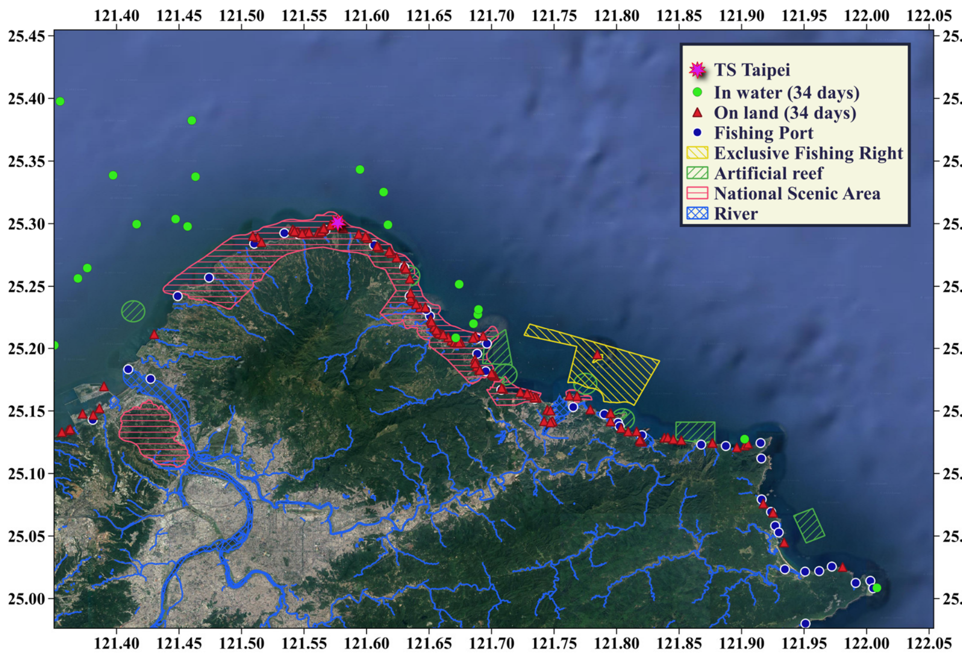

Figure 17. Risk map for the TS Taipei oil spill incident after 34 days.

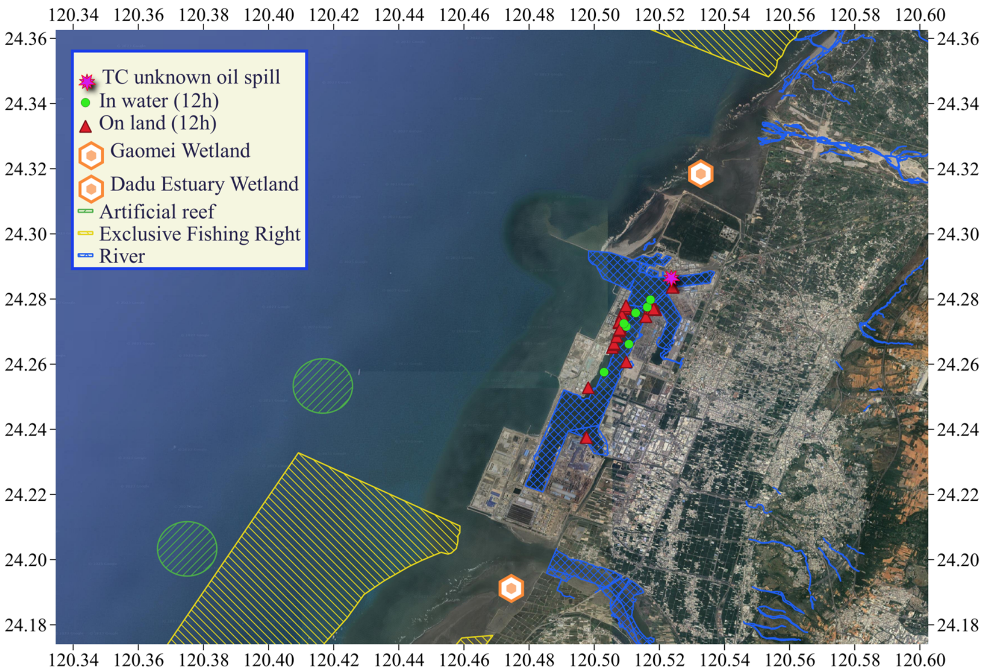

Figure 18. Risk map for the unknown oil spill incident in Taichung Port after 12 h.

In Figure 17, an oil spill risk map is presented, showing the situation 34 days after the TS Taipei incident, specifically for Case I. The map reveals that the entire northeast coast was impacted by oil slicks. Notably, the risk map indicates that the in-water oil slicks continued to expand and drift offshore, whereas the on-land oil slicks affected rivers, fishing ports, a national scenic area, an artificial fishing reef area, and an area subject to exclusive fishing rights.

Figure 18 displays another oil spill risk map for the unknown oil spill incident in Taichung Port, depicting the situation 12 h after the oil spill. The illustration highlights that the oil spill, under the influence of north-northeast monsoon winds, remained confined within the harbor. The oil slicks affected the rivers within the harbor while having no impact on the neighboring Gaomei Wetland.

The assessment of oil spill risk levels necessitates the analysis of various factors, such as manpower, aircraft, ships, transportation resources, weather conditions, and more. Furthermore, assessment methods differ across regions. Therefore, the development of oil spill risk level assessment indicators is a topic for future research and analysis. In subsequent studies, additional simulations can be conducted to model oil spill dispersion during different seasons, taking into account the influence of representative seasonal winds. The Environmental Sensitivity Index (ESI) provided by NOAA may also be utilized to generate risk maps and risk level indicators for each season. This approach would aid in assessing the vulnerability of various environmental areas to oil spills and prioritizing the allocation of limited response resources and efforts. By establishing a comprehensive emergency response plan based on these factors, the impact of oil spills on the marine environment and ecosystems can be swiftly controlled in the event of an incident.

5.2. Oil Spill Emergency Response

As previously discussed, oil spill incidents in coastal areas and harbors can have detrimental effects on the local marine environment, especially in ecologically sensitive areas. In order to effectively respond to such incidents, it is essential to establish a well-structured emergency response workflow that provides critical information to on-site response commanders, facilitating informed decision-making.

In this research, we propose a comprehensive workflow, as illustrated in Figure 19, which incorporates various tools and data adopted in our case studies. This workflow integrates numerical models, remote sensing technology, ocean-meteorological observational data, GIS, and geospatial information related to the marine environment and ecological sensitivity. Accessible through Google Earth on various devices and operating systems, this integrated workflow generates oil risk maps and provides crucial information, such as the oil spill extent and its impact on the marine environment, enabling more efficient development and execution of emergency response plans.

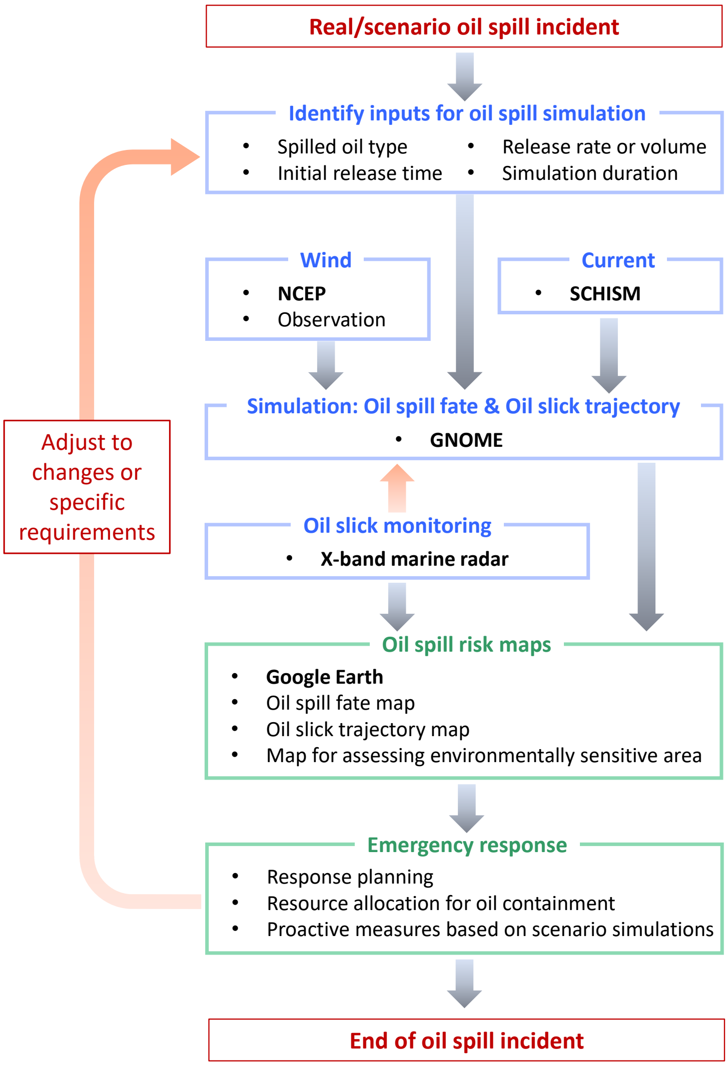

Figure 19. Proposed workflow for emergency response and oil containment resource allocation in cases of oil spill incidents occurring in coastal areas or within a harbor.

In addition to emergency response for actual oil spill incidents, it is also possible to proactively develop emergency plans for potential oil spill incidents by employing the proposed workflow for a variety of scenario simulations. It is worth noting that in Taiwan, this practice is regularly carried out by governmental agencies focused on marine environmental protection, such as the Ocean Conservation Administration, as well as by companies like CPC Taiwan and Formosa Plastics. These proactive emergency plans serve a dual purpose, enabling not only the swift facilitation of emergency responses but also the effective allocation of oil spill containment resources, including booms, skimmers, and dispersants.

5.3. Resource Allocation for Oil Spill Containment

In order to illustrate the allocation of resources for oil spill containment through the workflow, we considered the case of an unknown oil spill incident in Taichung Port. Figure 20 displays the risk map created 12 h after the incident. This map not only indicates the extent of oil slicks in the water and on land but also identifies four suggested deployment locations for oil containment booms: the northern entry of Taichung Port (Location A), the entrances of fishing ports (Locations B, C, and D), and the entrance to the tourist area (Location E). These locations have been strategically selected for their potential effectiveness in containing the oil spill. The deployment of oil containment booms is of paramount importance in responding to an oil spill incident. Utilizing the information used to create Figure 20, the boom length for each location can be readily determined.

Figure 20. Material allocation plan for containing the unknown oil spill incident in Taichung Port after 12 h (at 8:30 p.m. on 19 October 2018). The following locations are identified: A represents the northern entrance of Taichung Harbor; B, C, and D represent the entrances to the fishing port; and E represents the entrance to the tourist area.

For Location A, it is suggested to deploy an oil containment boom of 480 m in length, crucial for preventing the oil from spreading beyond the harbor and potentially affecting the sandy beach on the north side of Taichung Port, as illustrated in Figure 20. Locations B, C, and D require oil containment booms with suggested lengths of 200 m, 50 m, and 120 m, respectively. These boom lengths align with the widths of the entrances to the fishing ports. Finally, at Location E, which marks the narrowest part of the entrance to the tourist area, an oil containment boom of 90 m in length is advised to be deployed.

It is important to emphasize that this practice underscores the role of accurate simulation results, which are important in generating reliable oil risk maps that inform the planning and allocation of emergency response resources. Effective emergency response plans and resource allocation are essential for efficiently managing the spread of oil spills and for minimizing their impact on the marine environment and ecosystems.

6. Conclusions

A comprehensive workflow has been established for improving information management in the context of oil spill emergency response and resource allocation in the waters of Taiwan. This workflow consists of two primary components. The first component focuses on oil spill simulation, which is accomplished by utilizing observational data and various numerical tools. In this study, the numerical tools employed include SCHSIM for simulating ocean hydrodynamics, NCEP for wind simulation, and GNOME for oil dispersion simulation. It is noteworthy that the combination of SCHSIM and GNOME is demonstrated here for the first time. In order to demonstrate the effectiveness of the first component, two scenarios were considered: the TS Taipei oil spill incident under open sea conditions and an unknown oil spill incident in Taichung Port within a harbor area. The assessment reveals that the first component effectively works for both specific oil spill scenarios.

The second component of this workflow is dedicated to generating oil risk maps by merging the outcomes of the first component with specific geographical factors, including oil spill simulation results, environmental features, and ecologically sensitive areas, into Google Earth. By leveraging robust simulation tools, these oil spill risk maps for various time periods during the response phase of an oil spill event can be swiftly produced. These maps not only offer a visual representation of the risk information in affected marine areas but also aid on-site response commanders in promptly devising oil spill emergency response plans.

The workflow developed in this study can have broader applications, including the evaluation of potential oil incident scenarios and the creation of proactive emergency response plans. Furthermore, it facilitates the allocation of resources for containing oil slicks. It is important to note that while this workflow was primarily designed for addressing oil incidents in the waters of Taiwan, its adaptability and use can be extended to other locations with the open-source numerical tools employed in this study.

Author Contributions: Conceptualization, C.-M.C. and L.Z.-H.C.; methodology, C.-M.C. and W.-L.C.; software, C.-M.C. and Y.J.Z.; validation, C.-M.C.; formal analysis, C.-M.C., L.Z.-H.C. and Y.J.Z.; investigation, L.-C.W.; resources, W.-L.C., L.Z.-H.C. and C.-J.H.; data curation, C.-M.C. and L.-C.W.; writing—original draft preparation, C.-M.C.; writing—review and editing, W.-L.C., C.-J.H., L.Z.-H.C. and Y.J.Z.; visualization, C.-M.C.; supervision, W.-L.C.; project administration, W.-L.C.; funding acquisition, W.-L.C. All authors have read and agreed to the published version of the manuscript.

Funding: This research was funded by the National Science and Technology Council, Taiwan, NSTC 112-2636-E-110-007.

Institutional Review Board Statement: Not applicable.

Informed Consent Statement: Not applicable.

Data Availability Statement: Data will be made available on request.

Acknowledgments: We acknowledge the invaluable contribution of the Sciclone cluster at the College of William and Mary in facilitating the simulations presented in this paper. The simulations performed on the Sciclone cluster utilized the computational facilities provided by William & Mary Research Computing. For more information about these facilities, please visit their website at https://www.wm.edu/it/rc (accessed on 26 October 2023). Furthermore, acknowledgments to Taiwan's Central Weather Bureau and Harbor & Marine Technology Center for providing observational data to validate the numerical modeling.

Conflicts of Interest: The authors declare no conflict of interest.

References

1. Lehr, W.J. Review of modeling procedures for oil spill weathering behavior. *Adv. Ecol. Sci.* **2001**, *9*, 51–90.
2. Fingas, M. (Ed.) *Handbook of Oil Spill Science and Technology*; John Wiley & Sons: Hoboken, NJ, USA, 2014.
3. Reed, M.; Johansen, Ø.; Brandvik, P.J.; Daling, P.; Lewis, A.; Fiocco, R.; Prentki, R. Oil spill modeling towards the close of the 20th century: Overview of the state of the art. *Spill Sci. Technol. Bull.* **1999**, *5*, 3–16. [CrossRef]
4. Lehr, W.; Jones, R.; Evans, M.; Simecek-Beatty, D.; Overstreet, R. Revisions of the ADIOS oil spill model. *Environ. Model. Softw.* **2002**, *17*, 189–197. [CrossRef]
5. Spaulding, M.L. State of the art review and future directions in oil spill modeling. *Mar. Pollut. Bull.* **2017**, *115*, 7–19. [CrossRef] [PubMed]
6. Periáñez, R. A Lagrangian oil spill transport model for the Red Sea. *Ocean Eng.* **2020**, *217*, 107953. [CrossRef]

7. Liu, Z.; Chen, Q.; Zheng, C.; Han, Z.; Cai, B.; Liu, Y. Oil spill modeling of Chengdao oilfield in the Chinese Bohai Sea. *Ocean Eng.* **2022**, *255*, 111422. [CrossRef]
8. Proctor, R.; Flather, R.A.; Elliott, A.J. Modelling tides and surface drift in the Arabian Gulf—Application to the Gulf oil spill. *Cont. Shelf Res.* **1994**, *14*, 531–545. [CrossRef]
9. Guo, W.J.; Wang, Y.X. A numerical oil spill model based on a hybrid method. *Mar. Pollut. Bull.* **2009**, *58*, 726–734. [CrossRef]
10. Nordam, T.; Beegle-Krause, C.J.; Skancke, J.; Nepstad, R.; Reed, M. Improving oil spill trajectory modelling in the Arctic. *Mar. Pollut. Bull.* **2019**, *140*, 65–74. [CrossRef]
11. Chiu, C.M.; Huang, C.J.; Wu, L.C.; Zhang, J.Y.L.; Chang, L.Z.H.; Fan, Y.M.; Yu, H.C. Forecasting of oil-spill trajectories by using SCHISM and X-band marine radar. *Mar. Pollut. Bull.* **2018**, *137*, 566–581. [CrossRef]
12. Fingas, M. *Oil Spill Science and Technology*; Gulf Professional Publishing: Houston, TX, USA, 2016.
13. Fingas, M.; Brown, C.E. A review of oil spill remote sensing. *Sensors* **2017**, *18*, 91. [CrossRef] [PubMed]
14. Amir-Heidari, P.; Raie, M. Probabilistic risk assessment of oil spill from offshore oil wells in Persian Gulf. *Mar. Pollut. Bull.* **2018**, *136*, 291–299. [CrossRef] [PubMed]
15. Liubartseva, S.; Federico, I.; Coppini, G.; Lecci, R. Stochastic oil spill modeling for environmental protection at the Port of Taranto (southern Italy). *Mar. Pollut. Bull.* **2021**, *171*, 112744. [CrossRef] [PubMed]
16. Nelson, J.R.; Grubesic, T.H. Oil spill modeling: Risk, spatial vulnerability, and impact assessment. *Prog. Phys. Geogr. Earth Environ.* **2018**, *42*, 112–127. [CrossRef]
17. Barker, C.H.; Kourafalou, V.H.; Beegle-Krause, C.J.; Boufadel, M.; Bourassa, M.A.; Buschang, S.G.; Zheng, Y. Progress in operational modeling in support of oil spill response. *J. Mar. Sci. Eng.* **2020**, *8*, 668. [CrossRef]
18. Kankara, R.S.; Arockiaraj, S.; Prabhu, K. Environmental sensitivity mapping and risk assessment for oil spill along the Chennai Coast in India. *Mar. Pollut. Bull.* **2016**, *106*, 95–103. [CrossRef] [PubMed]
19. Skognes, K.; Johansen, Ø. Statmap-a 3-dimensional model for oil spill risk assessment. *Environ. Model. Softw.* **2004**, *19*, 727–737. [CrossRef]
20. Fernandes, R.; Necci, A.; Krausmann, E. *Model(s) for the Dispersion of Hazardous Materials in Floodwaters for RAPID-N, EUR 30968 EN*; European Union: Luxembourg, 2022; ISBN 978-92-76-46707-6. JRC127375.
21. Duran, R.; Romeo, L.; Whiting, J.; Vielma, J.; Rose, K.; Bunn, A.; Bauer, J. Simulation of the 2003 Foss barge-point wells oil spill: A comparison between BLOSOM and GNOME oil spill models. *J. Mar. Sci. Eng.* **2018**, *6*, 104. [CrossRef]
22. Zhang, Y.; Ye, F.; Stanev, E.V.; Grashorn, S. Seamless cross-scale modeling with SCHISM. *Ocean Model.* **2016**, *102*, 64–81. [CrossRef]
23. Ye, F.; Zhang, Y.; Friedrichs, M.; Wang, H.V.; Irby, I.; Shen, J.; Wang, Z. A 3D, cross-scale, baroclinic model with implicit vertical transport for the Upper Chesapeake Bay and its tributaries. *Ocean Model.* **2016**, *107*, 82–96. [CrossRef]
24. Ye, F.; Zhang, Y.J.; Wang, H.V.; Friedrichs, M.A.; Irby, I.D.; Alteljevich, E.; Valle-Levinson, A.; Wang, Z.; Huang, H.; Shen, J.; et al. A 3D unstructured-grid model for Chesapeake Bay: Importance of bathymetry. *Ocean Model.* **2018**, *127*, 16–39. [CrossRef]
25. Reed, M.; Turner, C.; Odulo, A. The role of wind and emulsification in modelling oil spill and surface drifter trajectories. *Spill Sci. Technol. Bull.* **1994**, *1*, 143–157. [CrossRef]
26. Spaulding, M.L.; Isaji, T.; Hall, P.; Allen, A.A. A hierarchy of stochastic particle models for search and rescue (SAR): Application to predict surface drifter trajectories using HF radar current forcing. *J. Mar. Sci. Eng.* **2006**, *8*, 181.
27. Lynch, D.R.; Greenberg, D.A.; Bilgili, A.; McGillicuddy, D.J., Jr.; Manning, J.P.; Aretxabaleta, A.L. *Particles in the Coastal Ocean: Theory and Applications*; Cambridge University Press: Cambridge, UK, 2015.
28. Farzingohar, M.; Zelina, Z.; Yasemi, M. Oil spill modelling of diesel and gasoline with GNOME around Rajaee port of Bandar Abbas, Iran. *Iran. J. Fish. Sci.* **2011**, *10*, 35–46.
29. Cheng, Y.; Li, X.; Xu, Q.; Garcia-Pineda, O.; Andersen, O.B.; Pichel, W.G. SAR observation and model tracking of an oil spill event in coastal waters. *Mar. Pollut. Bull.* **2011**, *62*, 350–363. [CrossRef] [PubMed]
30. Gurumoorthi, K.; Suneel, V.; Rao, V.T.; Thomas, A.P.; Alex, M.J. Fate of MV Wakashio oil spill off Mauritius coast through modelling and remote sensing observations. *Mar. Pollut. Bull.* **2021**, *172*, 112892. [CrossRef] [PubMed]
31. Zelenke, B.; O'Connor, C.; Barker, C.H.; Beegle-Krause, C.J. *General NOAA Operational Modeling Environment (GNOME) Technical Documentation*; GNOME: Seattle, WA, USA, 2012.
32. ITOPF (Oil Tanker Spill Statistics). The International Tanker Owners Pollution Federation. 2019. Available online: https://www.itopf.org/fileadmin/uploads/itopf/data/Documents/Company_Lit/Oil_Spill_Stats_brochure_2020_for_web.pdf (accessed on 26 October 2023).
33. Marta-Almeida, M.; Ruiz-Villarreal, M.; Pereira, J.; Otero, P.; Cirano, M.; Zhang, X.; Hetland, R.D. Efficient tools for marine operational forecast and oil spill tracking. *Mar. Pollut. Bull.* **2013**, *71*, 139–151. [CrossRef] [PubMed]
34. Zhang, Y.; Ateljevich, E.; Yu, H.-C.; Wu, C.H.; Yu, J.C.S. A new vertical coordinate system for a 3D unstructured-grid model. *Ocean Model.* **2015**, *85*, 16–31. [CrossRef]
35. Baptista, A.M. Solution of Advection-Dominated Transport by Eulerian–Lagrangian Methods Using the Backwards Method of Characteristics. Ph.D. Dissertation, MIT, Cambridge, MA, USA, 1987.
36. Roland, A.; Zhang, Y.J.; Wang, H.V.; Meng, Y.; Teng, Y.-C.; Maderich, V.; Brovchenko, I.; Dutour-Sikiric, M.; Zanke, U. A fully coupled 3D wave-current interaction model on unstructured meshes. *J. Geophys. Res. Oceans* **2012**, *117*. [CrossRef]
37. Schloen, J.; Stanev, E.V.; Grashorn, S. Wave-current interactions in the southern North Sea: The impact on salinity. *Ocean Model.* **2017**, *111*, 19–37. [CrossRef]

38. Chuang, L.Z.H.; Chiu, C.M.; Doong, D.J.; Huang, C.C.; Wu, L.C.; Fan, Y.M.; Huang, C.J.; Zhang, Y.J. Risk Assessment and Emergency Response Strategy of Oil Spills in Waters around Taiwan. *Mar. Res.* **2021**, *1*, 87–100.
39. Stolzenbach, K.; Madsen, O.S.; Adams, E.E.; Pollack, A.M. *A Review and Evaluation of Basic Techniques for Predicting the Behavior of Surface Oil Slicks*; Rep. 22; Department of Civil and Environmental Engineering, Massachusetts Institute of Technology: Cambridge, MA, USA, 1997.
40. GNOME. *General NOAA Operational Modeling Environment (GNOME) Technical Documentation. NOAA Technical Memorandum NOS OR&R 40*; GNOME: Seattle, WA, USA, 2012.
41. Prasad, S.J.; Balakrishnan Nair, T.M.; Rahaman, H.; Shenoi, S.S.C.; Vijayalakshmi, T. An assessment on oil spill trajectory prediction: Case study on oil spill off Ennore Port. *J. Earth Syst. Sci.* **2018**, *127*, 111. [CrossRef]
42. Saha, S.; Moorthi, S.; Wu, X.; Wang, J.; Nadiga, S.; Tripp, P.; Becker, E. The NCEP climate forecast system version 2. *J. Clim.* **2014**, *27*, 2185–2208. [CrossRef]
43. Yuan, X.; Wood, E.F.; Luo, L.; Pan, M. A first look at Climate Forecast System version 2 (CFSv2) for hydrological seasonal prediction. *Geophys. Res. Lett.* **2011**, *38*. [CrossRef]
44. Robbe, N.; Hengstermann, T. Remote sensing of marine oil spills from airborne platforms using multi-sensor systems. *Water Pollut. VIII Model. Monit. Manag.* **2006**, *1*, 347–355.
45. Zhu, X.; Li, Y.; Feng, H.; Liu, B.; Xu, J. Oil spill detection method using X-band marine radar imagery. *J. Appl. Remote Sens.* **2015**, *9*, 095985. [CrossRef]
46. Liu, P.; Li, Y.; Xu, J.; Zhu, X. Adaptive enhancement of X-band marine radar imagery to detect oil spill segments. *Sensors* **2017**, *17*, 2349. [CrossRef]
47. Dash, N. The use of geographic information systems in disaster research. *Int. J. Mass Emerg. Disasters* **1997**, *15*, 135–146. [CrossRef]
48. Ivanov, A.Y.; Zatyagalova, V.V. A GIS approach to mapping oil spills in a marine environment. *Int. J. Remote Sens.* **2008**, *29*, 6297–6313. [CrossRef]
49. Balogun, A.L.; Yekeen, S.T.; Pradhan, B.; Yusof, K.B.W. Oil spill trajectory modelling and environmental vulnerability mapping using GNOME model and GIS. *Environ. Pollut.* **2021**, *268*, 115812. [CrossRef]
50. Bucelli, M.; Paltrinieri, N.; Landucci, G. Integrated risk assessment for oil and gas installations in sensitive areas. *Ocean Eng.* **2018**, *150*, 377–390. [CrossRef]
51. D'Affonseca, F.M.; Reis, F.A.G.V.; dos Santos Corrêa, C.V.; Wieczorek, A.; do Carmo Giordano, L.; Marques, M.L.; Riedel, P.S. Environmental sensitivity index maps to manage oil spill risks: A review and perspectives. *Ocean Coast. Manag.* **2023**, *239*, 106590. [CrossRef]
52. Mohamadi, B.; Xie, Z.; Liu, F. GIS based oil spill risk assessment model for the Niger Delta's vegetation. *Nat. Environ. Pollut. Technol.* **2015**, *14*, 545.
53. Fan, C.; Hsu, C.J.; Lin, J.Y.; Kuan, Y.K.; Yang, C.C.; Liu, J.H.; Yeh, J.H. Taiwan's legal framework for marine pollution control and responses to marine oil spills and its implementation on TS Taipei cargo shipwreck salvage. *Mar. Pollut. Bull.* **2018**, *136*, 84–91. [CrossRef]
54. ITOPF. *TIP 01: Aerial Observation of Marine Oil Spills, Technical Information Paper*; ITOPF: Lodon, UK, 2014.
55. ITOPF. *TIP 02: Fate of Marine Oil Spills, Technical Information Paper*; ITOPF: Lodon, UK, 2014.
56. General NOAA. *Oil Modelling Environment (GNOME) User's Manual*; NOAA: Seattle, WA, USA, 2002.